INSTABILITY OF A WHIRLING CONDUCTING ROD IN THE PRESENCE OF A MAGNETIC FIELD

G.H.M. van der Heijden
Centre for Nonlinear Dynamics
University College London
London WC1E 6BT, UK
g.heijden@ucl.ac.uk

J. Valverde
Department of Mechanical Engineering
University of Seville
41092 Seville, Spain
jvalverde@us.es

Abstract

We study the effect of a magnetic field on the behaviour of a slender conducting elastic structure subject to end forces. Both statical (buckling) and dynamical (whirling) instability are considered and we also compute post-buckling configurations. The theory used is the geometrically exact Cosserat rod theory. We consider two types of boundary conditions: the traditional welded boundary conditions and a novel set of boundary conditions that give rise to exact helical post-buckling solutions. Our results are relevant for current designs of electrodynamic space tethers and potentially for future applications in nano- and molecular wires.

Key words

Conducting rod, magnetic field, Cosserat theory, bifurcation, helical solutions, space tether.

1 Introduction

A straight current-carrying wire held in tension between pole faces of a magnet is well known to buckle into a (roughly) helical configuration at a critical current (see Figure 1). A photograph of this phenomenon is shown in Section 10.4.3 of [Woodson and Melcher, 1968], where a linear stability analysis is carried out for a simple string model. (A string is here meant to be a perfectly flexible elastic wire.) The problem was studied in [Wolfe, 1983] by means of a rigorous bifurcation analysis for a (nonlinearly elastic) string suspended between fixed supports and placed in a uniform magnetic field directed parallel to the undeformed wire. He found that an infinite number of solution branches bifurcate from the trivial straight solution, much like in the Euler elastica under compressive load. In this case the non-trivial solutions are exact helices. That this should be so, is easily explained by the fact that the (Lorentz) body force is everywhere normal to the deformed configuration and hence the wire necessarily in a uniform state of tension. Some (statical) stability results (i.e., minimisation of the potential energy) could be obtained as well, indicating that the first branch of solutions is stable while the others are unstable.

In a subsequent paper [Wolfe, 1985] Wolfe extends the analysis to a uniformly rotating (whirling) string and shows again the existence of bifurcating branches of whirling non-trivial solutions. Due to centrifugal effects no closed-form solutions could be obtained in this case. This result was further extended in [Healey, 1990] using equivariant bifurcation theory in order to deal with the symmetries of the problem in the case of an isotropic rod.

Wolfe also considered a conducting *rod* in a uniform magnetic field [Wolfe, 1988]. In addition to extension a rod can undergo flexure, torsion and shear, and for the case of welded boundary conditions it was found that in certain cases bifurcation occurs, with the usual infinity of non-trivial equilibrium states. All the works cited above were content with showing the existence of bifurcating solutions and did not study their post-buckling behaviour.

The study of strings and rods in a magnetic field is of great interest to space tethers. Although space tethers in the last 20 years or so have become a well estab-

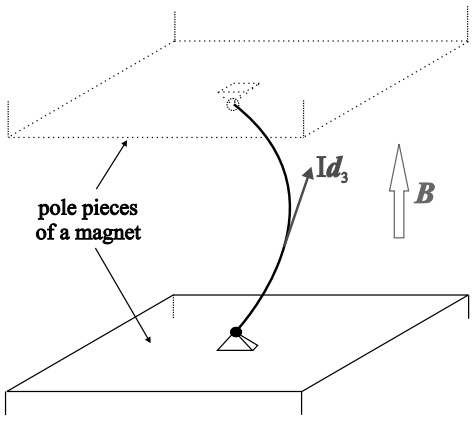

Figure 1. Experimental setup for a conducting wire.

lished concept in astrodynamics [Beletsky, 1993], new designs continue to be proposed that hold great potential for future space applications. A space tether is a long cable used to connect spacecraft to each other or to other orbiting bodies such as space stations, boosters, payload, etc. in order to transfer energy and momentum thus providing space propulsion without consuming propellant. These tethers have been studied as elastic strings (e.g., [Krupa *et al.*, 2000]) and as dumbbell systems (e.g., [Ziegler and Cartmell, 2001]). An important class of space tethers is formed by the so-called electrodynamic tethers (ETs). These employ the earth's magnetic field and ionospheric plasma to generate a current, according to Faraday's Law, and hence thrust or drag forces without expending chemical fuel. An example is the Short Electrodynamic Tether (SET) prototype of the European Space Agency [Valverde *et al.*, 2003]. This tether system, which comprises a central module from which two tethers each about a hundred metres long extend, is designed to operate at high inclination and in low orbit. Due to the shape of the earth's magnetic field this means that the desirable orientation of the tether is the horizontal one (i.e., with the axis of smallest moment of inertia normal to the orbit plane). The gravity gradient ordinarily causes a tether to drift to the stable radial position. Therefore, in order to keep the system in the horizontal position, an axial spin velocity is applied for gyroscopic stability. This requires significant torsional and bending rigidity of the tether which therefore has to be modelled as a rod, not a string. The applied spin causes large deformations that present stability issues similar to those in an unbalanced rotor system, which have been studied in previous work [Valverde *et al.*, 2005; Valverde *et al.*, 2005].

In this paper we apply large-deformation rod theory to study the effect of a magnetic field on the behaviour of a slender conducting elastic structure possibly subject to end forces. Both statical (buckling) and dynamical (whirling) instability are considered and we also compute post-buckling configurations. The work extends the stability analysis of the SET in [Valverde *et al.*, 2005] by including the effect of the magnetic field. This effect was considered small for the SET but that need not be true for other tether designs. For instance, very long and flexible tethers subject to boundary conditions that are not too restraining (e.g., no big end masses) might well operate in the region of the first magnetic buckling instability (we comment on this in Section 5).

We consider two types of boundary conditions. First the traditional welded boundary conditions. These are appropriate for tethers with sufficiently large attached end masses (see Figure 2). Wolfe considered welded boundary conditions in [Wolfe, 1988], where he also reports numerical evidence of helical post-buckling solutions. However, exact helical solutions cannot be supported by (coaxial) welded boundary conditions. Therefore we formulate novel 'coat hanger' boundary conditions that do support exact helical solutions, and show numerically that subject to these boundary conditions the rod does indeed buckle into a helix, or more precisely, that there is a (presumably infinite) series of helical modes bifurcating at increasing load, each successive mode having one more (half) helical turn. Unlike in string buckling the rod does not require a tensile force in the trivial state, but we allow for such an applied force as well. The pertinent dimensionless parameter that governs buckling measures the product of current and magnetic field against the bending force.

We also study steady whirling solutions for which we introduce a rotating co-ordinate system. This extends Wolfe's analysis of whirling strings to whirling rods. The results are important for the stability of spinning tether configurations. An interesting feature of helical solutions is that since all points on a helix have equal distance to the whirling axis, and are therefore equally affected by centrifugal forces, solutions remain helices when spun.

The paper is organised as follows. First, in Section 2, we give more details about the tether application and discuss the effect of the earth's magnetic field on an electrodynamic tether. Then we present our rod mechanics formulation in which the magnetic field enters the force balance equation through the Lorentz body force. For the study of whirling solutions the equilibrium equations are transformed to a co-ordinate system rotating at constant angular velocity. We use numerical bifurcation and continuation methods to find the buckling loads and to compute post-buckling solutions paths, both for the statical and dynamical case. These results are presented in the form of bifurcation diagrams in Section 5, first for welded and then for coat hanger boundary conditions. In Section 6, finally, we draw some conclusions and speculate on the relevance of our results for nano- and molecular wires.

2 Electrodynamic tethers and the earth's magnetic field

Electrodynamic tethers are electrical conductors that interact with the geomagnetic field in such a way that an electromotive force (e.m.f.) is generated along the tether due to Faraday's Law [Cosmo and Lorenzini, 1997]. The electrical circuit is closed by means of two contactors attached to the ends of the tether which interact with the surrounding ionospheric plasma and allow a current to flow.

Figure 2 shows an electrodynamic tether connecting two satellites. Let $\{\boldsymbol{i}, \boldsymbol{j}, \boldsymbol{k}\}$ be the orbital frame, which may be assumed to be inertial (since the angular velocity of the tether around the earth is much smaller than the typical spin velocity about its axis). The tether travels with a velocity $\boldsymbol{v}$ in the direction of $\boldsymbol{k}$. The e.m.f. between the ends induced by this motion is given by

$$E = \int_l (\boldsymbol{v} \times \boldsymbol{B}_0) \cdot \mathrm{d}\boldsymbol{l}, \tag{1}$$

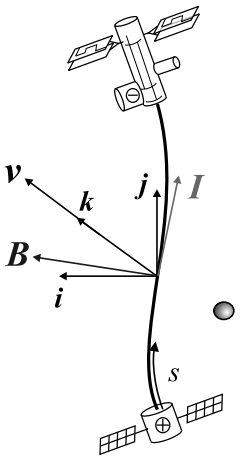

Figure 2. An electrodynamic tether in the earth's magnetic fi eld.

where $\boldsymbol{B}_0$ is the magnetic field and $d\boldsymbol{l}$ is a differential along the length of the tether. Because the tether is part of a closed circuit a current $\boldsymbol{I}$ will flow in the direction of increasing E and the system functions as a generator. This current in turn gives rise to a Lorentz force $\boldsymbol{F}_L$ through

$$\mathrm{d}\boldsymbol{F}_L = \mathrm{d}\boldsymbol{I} \times \boldsymbol{B}_0. \tag{2}$$

This force can be used to drag the system without expending chemical fuel [Cosmo and Lorenzini, 1997; Beletsky, 1993]. Alternatively, if a current is forced against the e.m.f. the system becomes a motor boosting itself to a higher orbit.

If we denote the position co-ordinates of the tether's central axis relative to $\{\boldsymbol{i}, \boldsymbol{j}, \boldsymbol{k}\}$ by (X, Y, Z), then the current vector, which is directed along the tangent of the tether, can be expressed as

$$\mathrm{d}\boldsymbol{I} = I\mathrm{d}\boldsymbol{l} = I\left(\frac{\partial X}{\partial s}, \frac{\partial Y}{\partial s}, \frac{\partial Z}{\partial s}\right)^T \mathrm{d}s. \tag{3}$$

The maximum force is generated when $\boldsymbol{I}$ and $\boldsymbol{B}_0$ are perpendicular. In the ET operation conditions both vectors will in general not be perpendicular because the tether is not perfectly straight and the magnetic field lines will not be perpendicular to the tether over its entire length. In order to represent this imperfection let us therefore assume that the magnetic field has an extra component in the Y direction

$$\boldsymbol{B}_0 = (B_1, B_2, 0)^T, \tag{4}$$

where $B_1 \gg B_2$. Introducing (3) and (4) into (2), the differential of the Lorentz force is found to be

$$\mathrm{d}\boldsymbol{F}_L = I\left(-\frac{\partial Z}{\partial s}B_2, \frac{\partial Z}{\partial s}B_1, \frac{\partial X}{\partial s}B_2 - \frac{\partial Y}{\partial s}B_1\right)^T \mathrm{d}s. \tag{5}$$

The term $-\frac{\partial Y}{\partial s}B_1 I\mathrm{d}s$ in the Z component opposes the motion and drags the ET system, as intended. However, the B_2 terms in the X and Z components (due to the imperfection B_2) will tend to coil the tether. This undesirable effect has been reported in some tether flights [Cosmo and Lorenzini, 1997; Beletsky, 1993].

In this paper we study the interaction of elastic and electromagnetic forces in a conducting rod and the tendency to generate three-dimensional coiled configurations (for instance as a result of buckling at critical loads).

3 The rod mechanics model

We describe the elastic behaviour of a conducting cable by the Kirchhoff equations for the dynamics of thin rods. The rod is assumed to be uniform, inextensible, unshearable and intrinsically straight and prismatic. For the background of the Kirchhoff equations the reader is referred to [Antman, 1995; Coleman *et al.*, 1993]. These equations were also used in [Valverde *et al.*, 2005] to analyse the dynamics of the SET. To these equations will be added the Lorentz force to account for the electromagnetic interaction.

Let $\boldsymbol{x}$ denote the position of the rod's centreline and let $\{\boldsymbol{d}_1, \boldsymbol{d}_2, \boldsymbol{d}_3\}$ be a right-handed orthonormal frame of directors (the Cosserat triad) defined at each point along the centreline. Since the centreline is assumed to be inextensible we can take $\boldsymbol{d}_3$ in the direction of the local tangent:

$$\boldsymbol{x}'(s,t) = \boldsymbol{d}_3(s,t), \tag{6}$$

where the prime denotes differentiation with respect to arclength s measured along the centreline, and t is time. The directors $\boldsymbol{d}_1$ and $\boldsymbol{d}_2$ will be taken to point along the principal bending axes of the cross-section (see Figure 3). The unstressed rod is taken to lie along the basis vector $\boldsymbol{k}$ of a fixed inertial frame $\{\boldsymbol{i}, \boldsymbol{j}, \boldsymbol{k}\}$.

Looking at Figure 3 we note that the position vector of an arbitrary point of the rod can be expressed as

$$\begin{aligned}\boldsymbol{X}(s, x_1, x_2, t) &= \boldsymbol{x}(s,t) + x_1\boldsymbol{d}_1(s,t) + x_2\boldsymbol{d}_2(s,t) \\ &= \boldsymbol{x}(s,t) + \boldsymbol{r}(s, x_1, x_2, t),\end{aligned} \tag{7}$$

where (x_1, x_2) are the components of $\boldsymbol{r}$ in the cross-section relative to $\{\boldsymbol{d}_1(s), \boldsymbol{d}_2(s)\}$. The rod is thus

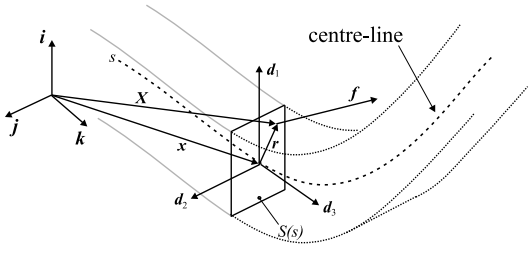

Figure 3. Cosserat model of a rod.

viewed as a set of infinitesimal slices centred at all s. A one-dimensional description will be obtained by averaging of forces and moments over each cross-section. The internal traction, which is the projection of the stress tensor onto the cross-sectional plane, is given by a force which we denote by $\boldsymbol{f} = \boldsymbol{f}(s, x_1, x_2, t)$ (see Figure 3). The resultant elastic force exerted in a section $S(s)$ is given by

$$\boldsymbol{F}(s,t) = \int_{S(s)} \boldsymbol{f}(s, x_1, x_2, t)\, \mathrm{d}S, \tag{8}$$

where $\mathrm{d}S$ is an infinitesimal area element. This force can be expressed in the director basis as $\boldsymbol{F} = \sum_{i=1}^{3} F_i\, \boldsymbol{d}_i$. The resultant moment in the section $S(s)$ is given by

$$\boldsymbol{M}(s,t) = \int_{S(s)} \boldsymbol{r}(s, x_1, x_2, t) \times \boldsymbol{f}(s, x_1, x_2, t)\, \mathrm{d}S, \tag{9}$$

and will be expressed as $\boldsymbol{M} = \sum_{i=1}^{3} M_i \boldsymbol{d}_i$.

The rod is assumed to carry an electric current for which we can write

$$\boldsymbol{I} = I\boldsymbol{x}' = I\boldsymbol{d}_3. \tag{10}$$

Here we have assumed the current to have the same direction as the rod, which is consistent with a one-dimensional rod theory. It amounts to the assumption that the cross-section of the conducting wire is small enough to make currents within the cross-section (eddy currents) induced by the motion negligible. The current $\boldsymbol{I}$ interacts with the magnetic field $\boldsymbol{B}_0$ to generate a (Lorentz) body force given by

$$\boldsymbol{F}_L = I\boldsymbol{d}_3 \times \boldsymbol{B}_0. \tag{11}$$

Following [Wolfe, 1983] we assume the magnetic field to be uniform and directed along the unstressed rod, i.e.,

$$\boldsymbol{B}_0 = B_0\boldsymbol{k}. \tag{12}$$

The balancing of forces and moments across an infinitesimal rod element then yields the following set of partial differential equations:

$$\boldsymbol{F}' + IB_0\boldsymbol{d}_3 \times \boldsymbol{k} = \rho A\ddot{\boldsymbol{x}}, \tag{13}$$

$$\boldsymbol{M}' + \boldsymbol{d}_3 \times \boldsymbol{F} = \rho(I_1\boldsymbol{d}_1 \times \ddot{\boldsymbol{d}}_1 + I_2\boldsymbol{d}_2 \times \ddot{\boldsymbol{d}}_2), \tag{14}$$

where ρ is the (volumetric) mass density, A the cross-sectional area, I_1 and I_2 the second moment of area of the cross-section about $\boldsymbol{d}_2$ and $\boldsymbol{d}_1$ respectively, and $\dot{()}$ denotes differentiation with respect to time.

For a closed system of equations these balance equations need to be supplemented by constitutive relations that characterise the material behaviour of the rod. We assume the rod to be made of homogeneous isotropic material and take the usual linear stress-strain relations (Hooke's law)

$$\begin{aligned} M_1 &= EI_1\kappa_1, \\ M_2 &= EI_2\kappa_2, \\ M_3 &= GJ\kappa_3, \end{aligned} \tag{15}$$

where κ_1 and κ_2 are the curvatures about $\boldsymbol{d}_1$ and $\boldsymbol{d}_2$, respectively, while κ_3 is the twist about $\boldsymbol{d}_3$. E is Young's modulus, G is the shear modulus and J is the second moment of area of the section about $\boldsymbol{d}_3$. We shall assume that the section is symmetric with respect to the principal axes, in which case $J = I_1 + I_2$.

The κ_i are the components of the curvature vector

$$\boldsymbol{\kappa} = \sum_{i=1}^{3} \kappa_i\, \boldsymbol{d}_i, \tag{16}$$

which governs the evolution in space of the frame of directors as one moves along the centreline:

$$\boldsymbol{d}_i' = \boldsymbol{\kappa} \times \boldsymbol{d}_i \qquad (i = 1, 2, 3). \tag{17}$$

The constitutive relations (15) can be used to replace the κ_i in (17) by moments, after which the equations (6), (13), (14) and (17) form a system of 18 differential equations for the 18 unknowns $(\boldsymbol{x}, \boldsymbol{F}, \boldsymbol{M}, \boldsymbol{d}_1, \boldsymbol{d}_2, \boldsymbol{d}_3)$.

Remark: In general when a conducting wire moves in a magnetic field an additional electromagnetic induction effect occurs which opposes the motion. The electromotive force as a result of this effect is proportional to the rate of change of the enclosed magnetic flux [Jackson, 1975]. However, in the case of a steadily whirling wire in a uniform magnetic field the enclosed magnetic flux does not change and the effect is zero.

3.1 Equations of motion in the moving frame

Since we are interested in steadily rotating solutions we transform the equilibrium equations (13) and (14) to a co-ordinate frame $\{\boldsymbol{e}_1, \boldsymbol{e}_2, \boldsymbol{e}_3\}$ that rotates with constant angular velocity $\boldsymbol{\omega} = \omega\boldsymbol{k}$ about the $\boldsymbol{k}$ axis (and the axis of the rod in its trivial unstressed state). Noting that the derivative with respect to time of an arbitrary vector $\boldsymbol{V}(s,t)$ is given by

$$\left.\frac{\mathrm{d}\boldsymbol{V}(s,t)}{\mathrm{d}t}\right|_i = \left.\frac{\mathrm{d}\boldsymbol{V}(s,t)}{\mathrm{d}t}\right|_m + \boldsymbol{\omega} \times \boldsymbol{V}(s,t), \tag{18}$$

where $\frac{\mathrm{d}}{\mathrm{d}t}\big|_i$ means derivative with respect to time in the inertial frame and $\frac{\mathrm{d}}{\mathrm{d}t}\big|_m$ expresses the derivative with respect to time in the moving frame, the equations (13) and (14) expressed relative to $\{\boldsymbol{e}_1, \boldsymbol{e}_2, \boldsymbol{e}_3\}$ become

$$\boldsymbol{F}' + IB_0\boldsymbol{d}_3 \times \boldsymbol{e}_3 = \rho A(\ddot{\boldsymbol{x}} + 2\boldsymbol{\omega} \times \dot{\boldsymbol{x}} + \boldsymbol{\omega} \times (\boldsymbol{\omega} \times \boldsymbol{x})), \tag{19}$$

$$\begin{aligned}\boldsymbol{M}' + \boldsymbol{d}_3 \times \boldsymbol{F} = \rho I_1(\boldsymbol{d}_1 \times \ddot{\boldsymbol{d}}_1 + 2\boldsymbol{d}_1 \times (\boldsymbol{\omega} \times \dot{\boldsymbol{d}}_1) \\ +(\boldsymbol{\omega} \cdot \boldsymbol{d}_1)(\boldsymbol{d}_1 \times \boldsymbol{\omega})) + \rho I_2(\boldsymbol{d}_2 \times \ddot{\boldsymbol{d}}_2 + \\ 2\boldsymbol{d}_2 \times (\boldsymbol{\omega} \times \dot{\boldsymbol{d}}_2) + (\boldsymbol{\omega} \cdot \boldsymbol{d}_2)(\boldsymbol{d}_2 \times \boldsymbol{\omega})).\end{aligned} \tag{20}$$

Steadily rotating (whirling) solutions satisfy the equations (13) and (14) with the dotted variables set to zero:

$$\boldsymbol{F}' + IB_0\boldsymbol{d}_3 \times \boldsymbol{e}_3 = \rho A\boldsymbol{\omega} \times (\boldsymbol{\omega} \times \boldsymbol{x}), \tag{21}$$

$$\begin{aligned}\boldsymbol{M}' + \boldsymbol{d}_3 \times \boldsymbol{F} = \rho I_1(\boldsymbol{\omega} \cdot \boldsymbol{d}_1)(\boldsymbol{d}_1 \times \boldsymbol{\omega}) + \\ \rho I_2(\boldsymbol{\omega} \cdot \boldsymbol{d}_2)(\boldsymbol{d}_2 \times \boldsymbol{\omega}).\end{aligned} \tag{22}$$

The other equations (6) and (17) do not change their form, but all vectors are now to be considered as expressed relative to the rotating frame $\{\boldsymbol{e}_1, \boldsymbol{e}_2, \boldsymbol{e}_3\}$. Statical solutions are simply obtained by setting ω equal to zero.

For a well-posed problem the final 18 ODEs require 18 boundary conditions to be specified. In the next two subsections we consider two cases.

3.2 Welded boundary conditions

We follow [Wolfe, 1988] and consider welded boundary conditions. These conditions also describe an electrodynamic tether that is welded to the end contactors or modules if these bodies are sufficiently massive (see Figure 2). We assume the rod to be fixed at $s = L$ and to be able to slide along $\boldsymbol{e}_3 = \boldsymbol{k}$ at $s = 0$ where a controlled force T is applied (positive for tension). L is the length of the rod. Writing $\boldsymbol{x} = x\boldsymbol{e}_1 + y\boldsymbol{e}_2 + z\boldsymbol{e}_3$ a consistent set of boundary conditions is thus given by

$$x(0) = 0, \tag{23}$$
$$y(0) = 0, \tag{24}$$
$$\boldsymbol{F}(0) \cdot \boldsymbol{e}_3 = -T, \tag{25}$$
$$\boldsymbol{d}_3(0) \cdot \boldsymbol{e}_1 = 0, \tag{26}$$
$$\boldsymbol{d}_3(0) \cdot \boldsymbol{e}_2 = 0, \tag{27}$$
$$\boldsymbol{d}_1(0) \cdot \boldsymbol{e}_2 = 0, \tag{28}$$

at $s = 0$ and

$$x(L) = 0, \tag{29}$$
$$y(L) = 0, \tag{30}$$
$$z(L) = L, \tag{31}$$
$$\boldsymbol{d}_3(L) \cdot \boldsymbol{e}_1 = 0, \tag{32}$$
$$\boldsymbol{d}_3(L) \cdot \boldsymbol{e}_2 = 0, \tag{33}$$
$$\boldsymbol{d}_1(L) \cdot \boldsymbol{e}_2 = 0, \tag{34}$$

at $s = L$. To these conditions we have to add conditions that ensure the orthonormality of the director basis, for which we can take

$$\begin{aligned}\boldsymbol{d}_1(0) \cdot \boldsymbol{d}_1(0) = 1, \\ \boldsymbol{d}_2(0) \cdot \boldsymbol{d}_2(0) = 1, \\ \boldsymbol{d}_3(0) \cdot \boldsymbol{d}_3(0) = 1, \\ \boldsymbol{d}_1(0) \cdot \boldsymbol{d}_2(0) = 0, \\ \boldsymbol{d}_1(0) \cdot \boldsymbol{d}_3(0) = 0, \\ \boldsymbol{d}_2(0) \cdot \boldsymbol{d}_3(0) = 0,\end{aligned} \tag{35}$$

for a total of 18 boundary conditions, as required. Note that these conditions imply that at $s = 0$ and $s = L$ the director frame $\{\boldsymbol{d}_1, \boldsymbol{d}_2, \boldsymbol{d}_3\}$ is aligned with $\{\boldsymbol{e}_1, \boldsymbol{e}_2, \boldsymbol{e}_3\}$.

3.3 Coat hanger boundary conditions

Helical solutions in rods are usually studied in infinitely long rods, which avoids the need for imposing boundary conditions. Indeed, it is not immediately clear how an exact helix can be supported: the boundary conditions cannot be simply welded as no two points on a helix have coaxial tangents, nor can they be simply pinned because a helix has curvature and therefore carries a bending moment. Here we formulate a set of boundary conditions that support exact helical solutions. We call them coat hanger boundary conditions, for obvious reasons.

Consider Figure 4 where a rod is suspended between two axes $\boldsymbol{v}_0$ (at $s = 0$) and $\boldsymbol{v}_1$ (at $s = 1$) lying in two parallel planes normal to $\boldsymbol{e}_3$. $\boldsymbol{v}_1$ is taken to be fixed in space, while $\boldsymbol{v}_0$ is free to move along $\boldsymbol{e}_3$. We assume the axes to have a fixed relative rotation ϕ, i.e., $\boldsymbol{v}_0 \cdot \boldsymbol{v}_1 = \cos\phi$. The rod is free to hinge about and slide along both $\boldsymbol{v}_0$ and $\boldsymbol{v}_1$. This situation is described by

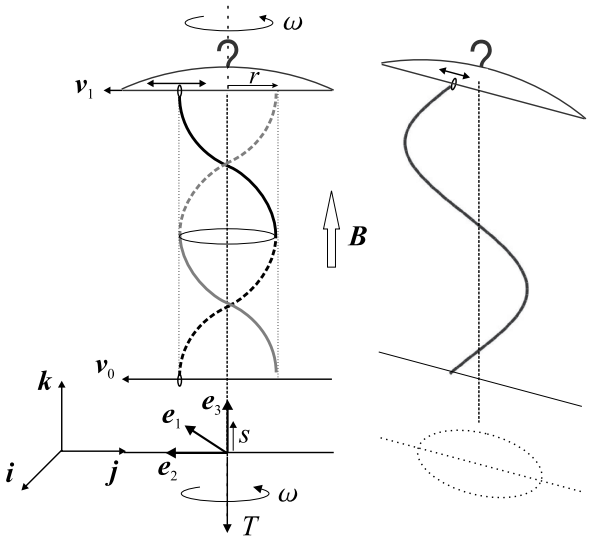

Figure 4. Coat hanger boundary conditions.

the following boundary conditions:

$$\boldsymbol{d}_1(0)\cdot\boldsymbol{v}_0=0, \tag{36}$$
$$\boldsymbol{d}_3(0)\cdot\boldsymbol{v}_0=0, \tag{37}$$
$$\boldsymbol{M}(0)\cdot\boldsymbol{v}_0=0, \tag{38}$$
$$\boldsymbol{F}(0)\cdot\boldsymbol{v}_0=0, \tag{39}$$
$$\boldsymbol{F}(0)\cdot\boldsymbol{e}_3=-T, \tag{40}$$
$$\boldsymbol{x}(0)\cdot(\boldsymbol{v}_0\times\boldsymbol{e}_3)=0, \tag{41}$$

at $s=0$, and

$$\boldsymbol{d}_1(L)\cdot\boldsymbol{v}_1=0, \tag{42}$$
$$\boldsymbol{d}_3(L)\cdot\boldsymbol{v}_1=0, \tag{43}$$
$$\boldsymbol{M}(L)\cdot\boldsymbol{v}_1=0, \tag{44}$$
$$\boldsymbol{x}(L)\cdot(\boldsymbol{v}_1\times\boldsymbol{e}_3)=0, \tag{45}$$
$$\boldsymbol{x}(L)\cdot\boldsymbol{v}_1=r, \tag{46}$$
$$z(L)=L, \tag{47}$$

at $s=1$. T is an applied end force (positive for tension). To ensure orthonormality of the director basis we again add

$$\begin{aligned}
&\boldsymbol{d}_1(0)\cdot\boldsymbol{d}_1(0)=1,\\
&\boldsymbol{d}_2(0)\cdot\boldsymbol{d}_2(0)=1,\\
&\boldsymbol{d}_3(0)\cdot\boldsymbol{d}_3(0)=1,\\
&\boldsymbol{d}_1(0)\cdot\boldsymbol{d}_2(0)=0,\\
&\boldsymbol{d}_1(0)\cdot\boldsymbol{d}_3(0)=0,\\
&\boldsymbol{d}_2(0)\cdot\boldsymbol{d}_3(0)=0,
\end{aligned} \tag{48}$$

completing the set of boundary conditions.

These conditions describe a rod that is hinged about $\boldsymbol{d}_2$ at both ends. Conditions (41) and (45) restrict the movement of the ends of the rod to the planes spanned by $(\boldsymbol{v}_0,\boldsymbol{e}_3)$ and $(\boldsymbol{v}_1,\boldsymbol{e}_3)$, respectively. Condition (46) requires some explanation. A helix is a curve of constant axial radius r and (total) curvature $\kappa=\sqrt{\kappa_1^2+\kappa_2^2}$. The two are related according to $\kappa r=\sin^2\theta$, where θ is the helical angle defined by $\boldsymbol{d}_3\cdot\boldsymbol{e}_3=\cos\theta$ if $\boldsymbol{e}_3$ is along the axis of the helix (the angle $\frac{\pi}{2}-\theta$ is usually called the pitch angle). Since the rod is hinged about $\boldsymbol{d}_2$, we have $\kappa_2=0$. So, in order to support helical solutions we can take for r in (46) the expression

$$r=\frac{1-(\boldsymbol{d}_3\cdot\boldsymbol{e}_3)^2}{\kappa_1}. \tag{49}$$

Note that here κ_1 can be taken with its sign, so that (46) also specifies which way the rod moves along $\boldsymbol{v}_1$. When the rod buckles, the axis $\boldsymbol{v}_0$ lifts up and the rod is free to find its own radius r. Condition (46) ensures that any bifurcating helices will be centred at $\boldsymbol{e}_3$. This is important when we start rotating the axes $\boldsymbol{v}_0$ and $\boldsymbol{v}_1$ about $\boldsymbol{e}_3$. A centred helix will experience a uniform centrifugal force and is therefore expected to remain helical.

We shall take $\phi=0$ so that the initial rod, lying straight along $\boldsymbol{e}_3$, is untwisted. This choice implies that any helices will have an integer number of half helical periods. Also, the directors, and hence the cross-section of the rod, will make a half-integer number of turns between $s=0$ and $s=L$. Note that in this case of aligned $\boldsymbol{v}_0$ and $\boldsymbol{v}_1$ boundary condition (46) also prevents a rigid body translation along these axes. Without loss of generality we may choose $\boldsymbol{v}_0=\boldsymbol{v}_1=\boldsymbol{e}_2$, so that at the ends the directors $\{\boldsymbol{d}_1,\boldsymbol{d}_2,\boldsymbol{d}_3\}$ are aligned with $\{\boldsymbol{e}_1,\boldsymbol{e}_2,\boldsymbol{e}_3\}$.

Of course the above coat hanger boundary conditions merely *allow* helical solutions. They need not exist. However, if the equilibrium equations do have helical solutions and one-parameter curves of such solutions intersect the trivial path of straight solutions, then one might expect to detect them as (pitchfork) bifurcations at critical buckling loads. The results presented in Section 5 show that this is indeed the case.

4 Nondimensionalisation

We make the system of equations dimensionless by scaling the variables in the following way

$$\begin{aligned}
&\omega_c=\sqrt{f\frac{EI_1}{\rho AL^4}},\quad \bar{t}=t\omega_c,\quad \bar{s}=\frac{s}{L}\in[0,1],\\
&\bar{\boldsymbol{x}}=\frac{\boldsymbol{x}}{L},\quad \bar{\boldsymbol{F}}=\boldsymbol{F}\frac{L^2}{fEI_1},\quad \bar{T}=T\frac{L^2}{fEI_1},\\
&\bar{\omega}=\frac{\omega}{\omega_c},\quad \bar{\boldsymbol{M}}=\boldsymbol{M}\frac{AL^3}{fEI_1^2},\quad \bar{\boldsymbol{\kappa}}=\boldsymbol{\kappa}L.
\end{aligned} \tag{50}$$

Here ω_c is a reference bending natural frequency which, through tuning of the numerical constant f, can be adapted to the particular boundary conditions at hand and the natural mode considered. In the ET case, we take $f=500.5639$, which corresponds to the first bending natural frequency of a fixed-fixed beam about $\boldsymbol{d}_1$. In the case of the coat hanger boundary conditions we simply take $f=1$.

With this nondimensionalisation the equations become (dropping the overbars for simplicity and letting a prime denote $\frac{d}{d\bar{s}}$):

$$\boldsymbol{F}'+B\boldsymbol{d}_3\times\boldsymbol{k}=\boldsymbol{\omega}\times(\boldsymbol{\omega}\times\boldsymbol{x}), \tag{51}$$
$$\boldsymbol{M}'+Q\boldsymbol{d}_3\times\boldsymbol{F}=(\boldsymbol{\omega}\cdot\boldsymbol{d}_1)(\boldsymbol{d}_1\times\boldsymbol{\omega})+R(\boldsymbol{\omega}\cdot\boldsymbol{d}_2)(\boldsymbol{d}_2\times\boldsymbol{\omega}), \tag{52}$$
$$\boldsymbol{x}'=\boldsymbol{d}_3, \tag{53}$$
$$\boldsymbol{d}_i'=\boldsymbol{\kappa}\times\boldsymbol{d}_i, \tag{54}$$

and the constitutive relations can be written as

$$\boldsymbol{M} = \frac{Q}{f}\left[\kappa_1 \boldsymbol{d}_1 + R\kappa_2 \boldsymbol{d}_2 + \frac{\Gamma(1+R)}{2}\kappa_3 \boldsymbol{d}_3\right], \quad (55)$$

where the dimensionless parameters are

$$Q = \frac{AL^2}{I_1}, \quad R = \frac{I_2}{I_1}, \quad B = \frac{B_0 I L^3}{f E I_1}, \quad \Gamma = \frac{2G}{E}. \quad (56)$$

$\frac{1}{\Gamma} - 1$ is equal to Poisson's ratio. For the boundary conditions we can still use (23) to (48) if we assume that they now refer to dimensionless variables and that the right-hand conditions are imposed at $\bar{s} = 1$.

5 Numerical results

We use the well-tested code AUTO [Doedel *et al.*, 1997] to compute single-parameter curves of solutions to the boundary-value problems formulated in Section 3. AUTO employs orthogonal collocation allied to pseudo-arclength continuation. It requires a starting solution and can then trace out solution curves as a parameter of the problem is varied. Bifurcations are detected where branches of solutions intersect. We start from the trivial straight and untwisted rod

$$\begin{aligned} &\bar{\boldsymbol{x}}(\bar{s}) = \bar{s}\boldsymbol{e}_3, \quad \bar{\boldsymbol{F}}(\bar{s}) = -\bar{T}\boldsymbol{e}_3, \quad \bar{\boldsymbol{M}}(\bar{s}) = \boldsymbol{0}, \\ &\boldsymbol{d}_i(\bar{s}) = \boldsymbol{e}_i \quad (i = 1, 2, 3), \quad \bar{s} \in [0, 1], \end{aligned} \quad (57)$$

which is a solution for both the welded and the coat hanger boundary conditions. The parameters we vary are B and ω.

5.1 Results for welded boundary conditions

Figure 5 shows the bifurcation diagram obtained when the magnetic field parameter B is varied, using a suitable phase-space norm along the vertical axis. The dimensionless parameters taken are those of the SET. They are listed in Table 1, along with the dimensional parameters. Note that ω is non-zero, so we are considering whirling solutions. The value of $\omega = 2$ has been chosen because spinning tethers generally operate above their first bending natural frequency [Tyc *et al.*, 1993; Valverde *et al.*, 2003]. We find a (presumably infinite) sequence of non-trivial branches bifurcating from the trivial (horizontal) branch at pitchfork bifurcations, similar to the case of a statical rod in a magnetic field [Wolfe, 1988]. Figure 5 shows the first six branches. They come in close pairs because of the relatively small anisotropy of the rod. The enlargement in Figure 5 reveals a solution branch connecting branches b1 and b2. A similar connection occurs between the pairs b3, b4 and b5, b6. The shapes of the rod along these connections form a smooth transition between the shapes on the connected branches.

L	$100\ m$	Q	9997136842.15
A	$4.16 \times 10^{-6}\ m^2$	R	0.5526
E	$1.32 \times 10^{11}\ \frac{N}{m^2}$	Γ	0.76923
EI_1	$38\ Nm^2$	f	500.5639
EI_2	$21\ Nm^2$		

Table 1. Dimensional and dimensionless parameters for the SET.

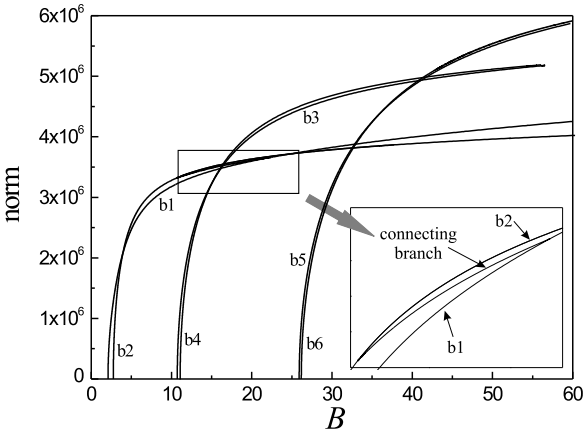

Figure 5. Bifurcation diagram for welded boundary conditions ($\omega = 2$).

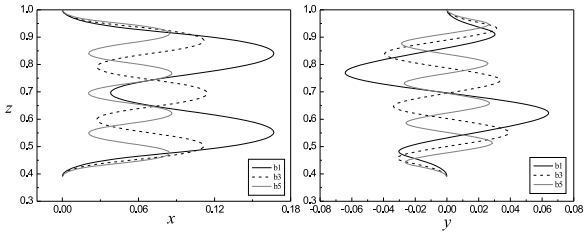

Figure 6. Projection of the first three modes onto the x-z and y-z planes at a constant $z(0) = 0.39$. Values of B are: 4.448 (b1), 16.49 (b3) and 38.74 (b5).

Projections onto x-z and y-z planes of bifurcating solutions along branches b1, b3 and b5 are shown in Figure 6 for constant $z(0) = 0.39$. Figure 7 shows the three-dimensional shape of a solution on the fourth bifurcating branch.

If the problem of the ET is treated from a design point of view, it would be interesting to quantify the value for which the ET buckles out of the trivial solution due to the action of the geomagnetic field. In the case at hand, this value is $B = 2.09$, which in dimensional variables would be $IB_0 = 7.942 \times 10^{-5}\ \frac{N}{m}$. Noting that the maximum value of the geomagnetic field is $B_g = 7 \times 10^{-5}\ T$ [Cosmo and Lorenzini, 1997], and assuming that the maximum current that will flow along the tether would be $I = 1\ A$ [Cosmo and Lorenzini, 1997], the maximum expected value for the constant $IB_g = 7 \times 10^{-5}\ \frac{N}{m}$. In our case, the ET would

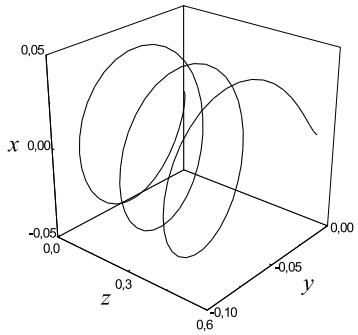

Figure 7. 3D view of a solution along b4.

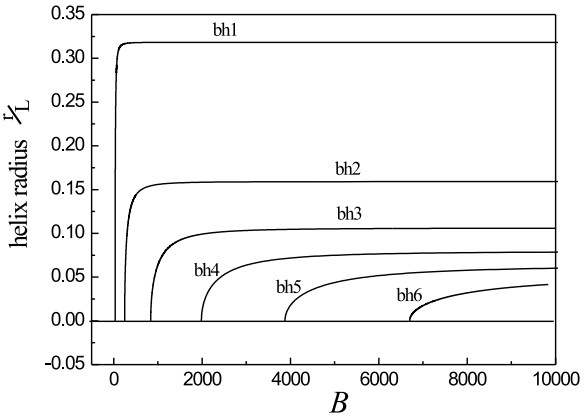

Figure 8. Bifurcation diagram for coat hanger boundary conditions ($\omega = 0$).

be below the critical value at any time but quite close to it. Note, though, that B goes as the cube of L and for longer tethers, which are common in radially stabilised ETs, the critical value may be exceeded resulting in buckling into a helical-like shape (cf. Figure 7), as has been reported in some tether flights, such as the PGM and TSS-1R missions [Beletsky, 1993; Cosmo and Lorenzini, 1997].

5.2 Results for coat hanger boundary conditions

First we consider the statical case ($\omega = 0$). The formulation of the boundary conditions in Section 3.3 is valid for anisotropic rods, but it turns out that perfect helices only occur for isotropic rods ($R = 1$). This is not surprising as it is well-known that for anisotropic rods the twist κ_3 (and hence the moment M_3) is not constant and therefore we should not expect uniform solutions. The values for the other parameters are given in Table 2. A bifurcation diagram is shown in Figure 8. Since bifurcating solutions are exact helices, the dimensionless helical radius r/L is plotted against B. A slight complication in computing this diagram occurs because of the denominator in (49), which is zero for the straight rod. However, this problem is easily resolved by replacing boundary condition (46) by $\boldsymbol{x}(L) \cdot \boldsymbol{v}_1 = 0$ along the trivial branch and switching back to (46) once an incipient non-trivial solution has been obtained.

Figure 9 shows x-z and y-z projections of bifurcating solutions along the first four branches, taken at constant curvature $\bar{\kappa} = 8$. It was noted in Section 3.3 that the coat hanger boundary conditions with $\phi = 0$ (i.e., parallel end supports $\boldsymbol{v}_0$ and $\boldsymbol{v}_1$) only allow helices of a half-integer number of helical turns. It turns out that each successive bifurcating solution in Figure 8 has one

L	$5\ m$	Q	8333333.33
A	$3 \times 10^{-5}\ m^2$	R	1
E	$30 \times 10^9\ \frac{N}{m^2}$	Γ	0.76923
$I_1 = I_2$	$9 \times 10^{11}\ m^4$	f	1

Table 2. Parameters used for the coat hanger boundary conditions.

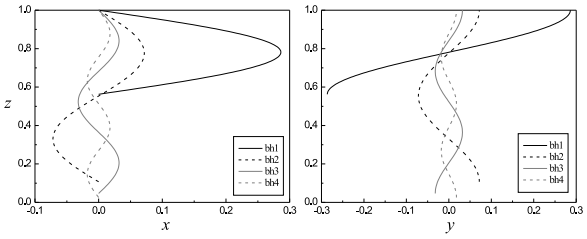

Figure 9. x-z and y-z projections of the first 4 helical modes at constant curvature $\kappa = 8$. Values of B are: 61.68 (bh1), 270.69 (bh2), 868.72 (bh3) and 2024.70 (bh4).

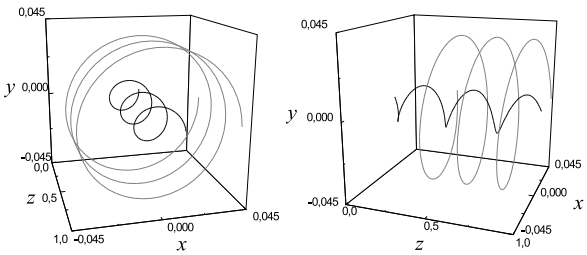

Figure 10. 3D views of helices on branch bh6.

more half helical turn. The bifurcating branches have handedness. That is, regardless of the sign of r, the bifurcating solutions are right-handed helices if, as here, $B > 0$ and would be left-handed helices if $B < 0$, i.e., had we run B in the other direction. Figure 10 shows three-dimensional views of a solution along the sixth branch. It has three full turns and nicely illustrates the exact helical shape.

Next we consider whirling motions in which the supports $\boldsymbol{v}_0$ and $\boldsymbol{v}_1$ are spun about $\boldsymbol{k}$ with constant angular velocity ω. Solutions remain helical, as expected, and Figures 11 and 12 show the effect of ω on a solution taken on the second branch of Figure 8.

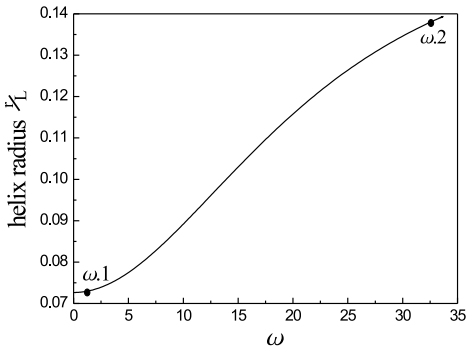

Figure 11. Influence of ω on the helical radius for a solution taken from the second branch bh2 with $B = 271.69$.

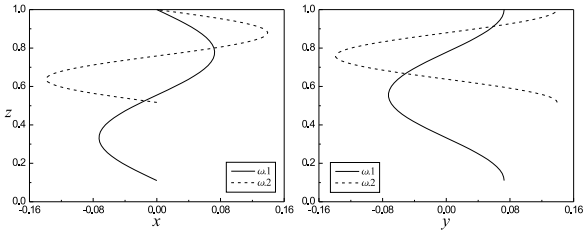

Figure 12. Projections of helical shapes for two solutions indicated in Figure 11.

6 Conclusions

We have shown that whirling current-carrying rods bifurcate under increasing magnetic field (or current). In the case of an isotropic rod the coat hanger boundary conditions that we introduced generate branches of exact helical solutions. The S^1 symmetry of this case (rotational symmetry about the $\boldsymbol{e}_3$ axis) complicated Wolfe's analysis of the whirling string [Wolfe, 1985]. Our coat hanger boundary conditions break the S^1 symmetry down to Z_2 symmetry (reflection symmetry along $\boldsymbol{v}_0$ and $\boldsymbol{v}_1$), and no problems in the application of standard results from bifurcation theory should arise. Indeed, the bifurcations are detected numerically in Figure 8 without difficulty.

Wolfe's analysis for strings suggests that the first bifurcating branch is stable and that all other branches are unstable. We expect the same to be true for rods but our present analysis does not give (dynamical) stability information. We intend to take up a stability analysis elsewhere.

We finally like to speculate on another possible application of this work. There is great current interest in conducting nanowires. These can either be silicon-based wires, carbon nanotubes or metal-coated biological fibres such as proteins, DNA molecules and microtubules [Scheibel *et al.*, 2003]. In addition there is the ongoing discussion whether or not DNA molecules are electrical conductors [Maiya and Ramasarma, 2001]. All these nanometer-scale structures are believed to have great potential as building blocks for future electronic devices. The interaction of these wires with magnetic fields could conceivably be exploited to obtain certain desirable properties.

References

Antman, S.S. (1995). *Nonlinear Problems of Elasticity*. Springer-Verlag, Berlin.

Beletsky V.V. and Levin, E.M. (1993). *Dynamics of Space Tether Systems*, Advances in the Astronautical Sciences Volume 83. American Astronautical Society.

Coleman, B.D., Dill, E.H., Lembo, M., Lu, Z. and Tobias, I. [1993] On the dynamics of rods in the theory of Kirchhoff and Clebsch, *Arch. Rat. Mech. Anal.* **121**, pp. 339–359.

Cosmo, M.L. and Lorenzini, E.C. (1997). *Tethers in Space Handbook*, 3rd edition. Smithsonian Astrophisical Observatory (NASA Marshall Space Flight Center).

Doedel, E.J., Champneys, A.R., Fairgrieve, T.R., Kuznetsov, Yu.A., Sandstede, B. and Wang, X.J. (1997). *AUTO97: Continuation and bifurcation software for ordinary differential equations* (available by anonymous ftp from `ftp.cs.concordia.ca/pub/doedel/auto`).

Healey, T.J. [1990] Large rotating states of a conducting elastic wire in a magnetic field: subtle symmetry and multiparameter bifurcation, *J. Elasticity* **24**, pp. 211–227.

Jackson, J.D. (1975). *Classical Electrodynamics*, 2nd edition. John Wiley & Sons, New York.

Krupa, M., Kuhn, A., Poth, W., Schagerl, M., Steindl, A., Steiner, W., Troger, H. and Wiedermann, G. [2000] Tethered satellite systems: A new concept of space flight, *Eur. J. Mech. A Solids* **19**, S145164.

Maiya, B.G. and Ramasarma, T. [2001] DNA, a molecular wire or not – The debate continues, *Current Science* **80**(12), pp. 1523–1530.

Tyc, G., Han, R.P.S., Vigneron, F.R., Jablonski, A.M., Modi, V.J. and Misra, A.K. [1993] Dynamics and stability of a spinning tethered spacecraft with flexible appendages, *Advances in the Astronautical Sciences* **85**(1), pp. 877–896.

Scheibel, T., Parthasarathy, R., Sawicki, G., Lin, X.M., Jaeger H. and Lindquist, S.L. [2003] Conducting nanowires built by controlled self-assembly of amyloid fibers and selective metal deposition, *Proc. Nat. Acad. Sci. USA* **100**, pp. 4527–4532.

Valverde, J., Escalona, J.L., Mayo J. and Domínguez, J. [2003] Dynamic analysis of a light structure in outer space: Short Electrodynamic Tether, *Multibody System Dynamics* **10**(1), pp. 125–146.

Valverde, J., Escalona, J.L., Freire E. and Domínguez, J. [2005] Stability and bifurcation analysis of a geometrically nonlinear orthotropic Jeffcott model with internal damping, *Nonlinear Dynamics* (in the press).

Valverde, J., Escalona, J.L., Domínguez, J. and Champneys, A. [2005] Stability and bifurcation analysis of the short electrodynamic tether; a geometrically non-

linear approach, submitted to *Journal of Nonlinear Science*.

Vigneron, F.R., Jablonski, A.M., Chandrashaker, R. and Tyc, G. [1997] Damped gyroscopic modes of spinning tethered space vehicles with flexible booms, *Journal of Spacecraft and Rockets* **34**(5), pp. 662–669.

Wolfe, P. [1983] Equilibrium states of an elastic conductor in a magnetic field: A paradigm of bifurcation theory, *Trans. Am. Math. Soc*. **278**, pp. 377–387.

Wolfe, P. (1985). Rotating states of an elastic conductor, in: *Physical Mathematics and Nonlinear Partial Differential Equations*, Lightbourne, J. and Rankin, S. (eds). Dekker, New York.

Wolfe, P. [1988] Bifurcation theory of an elastic conductingrod in a magnetic field, *Quart. J. Mech. Appl. Math.*, **41**(2), pp. 265–279.

Woodson H.H. and Melcher, J.R. (1968). *Electromechanical Dynamics, Part II: Fields, Forces, and Motion*. John Wiley & Sons, New York.

Ziegler S.W. and Cartmell, M.P. [2001] Using motorized tethers for payload orbital transfer, *Journal of Spacecraft and Rockets* **38**, pp. 904–913.